Live-Cell Imaging

DOI: 10.1002/ange.201100934

Near-Infrared-Fluorescence-Enhanced Molecular Imaging of Live Cells on Gold Substrates**

*Guosong Hong, Scott M. Tabakman, Kevin Welsher, Zhuo Chen, Joshua T. Robinson, Hailiang Wang, Bo Zhang, and Hongjie Dai**

Biological imaging in the near-infrared (NIR) region has the advantages of deep photon penetration as a result of the relatively high transparency, reduced scattering, and low autofluorescence of biological tissues in the 0.8 to 1.4 μm range.[1–5] Organic dyes,[6–9] quantum dots,[10–12] and single-walled carbon nanotubes (SWNTs)[4] have been employed for in vitro and in vivo biological imaging in the NIR region. SWNTs are a group of one-dimensional (1D) macromolecular fluorophores with intrinsic bandgap fluorescence emission between 0.9 and 1.4 μm upon excitation in the visible or NIR region.[4,13,14] The large Stokes shift makes SWNTs ideal probes for biological imaging with high contrast and low background.[3] Thus far, SWNTs have been used as fluorescence tags for in vitro cell imaging,[15,16] ex vivo imaging of tissues and organs,[17,18] and in vivo imaging of normal organs as well as tumors.[19,20]

A common caveat of NIR fluorophores is their relatively low quantum yield compared to that of their counterparts (including organic dyes and quantum dots) with shorter emission wavelengths in the visible, which limits their imaging capabilities. For example, the IR800 dye (with a peak emission wavelength at 800 nm) exhibits a quantum yield of about 10%,[21] and the indocyanine green (ICG) dye exhibits a quantum yield of only about 4.3% at an emission wavelength of 805 nm.[22] In contrast, molecules fluorescing at shorter wavelengths typically exhibit much higher quantum yields (IR700 about 24% at 700 nm emission,[21] cyanine-5 about 30% at 660 nm emission,[23] and fluorescein about 91%[24] at 521 nm emission). SWNTs exhibit quantum yields ranging from 0.1 to 3%[13,25,26] caused by intrinsic low-energy excitons that are optically forbidden,[27] extrinsic quenchers such as metallic SWNTs in bundles,[25] and oxygen in acidic environment.[28,29] To fully utilize the spectral advantages of NIR fluorophores, it is desirable to develop a general approach to enhancing the photoluminescence (PL) in the NIR, thus enhancing the capability of biological imaging in this important spectral region.

Recently, we reported metal-enhanced fluorescence (MEF) by up to 14-fold for surfactant-coated SWNTs deposited on nanostructured gold films synthesized solely in the solution phase by growing gold nanoparticles on gold seeds("Au/Au films").[30] Here, we employed the Au/Au substrate for NIR-fluorescence-enhanced (NIR-FE) cellular imaging by using both SWNTs and organic fluorescent labels. We used SWNTs functionalized by the arginine–glycine–aspartic acid (RGD) sequence to selectively tag U87-MG brain cancer cells over MCF-7 breast cancer cells, plated the cells on the Au/Au substrate, and observed an about ninefold increase in the fluorescence of the SWNT on U87-MG cells. We performed high-quality NIR molecular imaging of molecularly targeted cells by using much shorter exposure times (about 300 ms) than previously possible with nanotube fluorophores. With NIR-FE imaging, we were able to push the detectable limit of SWNT staining of cells down to an ultralow concentration of about 50 pM. Further, we observed different degrees of fluorescence enhancement for endocytosed, intracellular SWNTs in comparison to that of nanotubes on the cell membrane at the cell/gold interface; this finding suggests the possibility of observing transmembrane endocytosis of live cells based on the degree of fluorescence enhancement.

Our NIR-FE imaging method of biological systems is general for commonly used low-quantum-yield organic dyes including IR800. To the best of our knowledge, this is the first report of the fluorescence-enhanced imaging of cells on Au nanostructures in the NIR region. Previously, Ag substrates were used for fluorescence-enhanced biological imaging in the visible region with organic dyes.[31–33]

Cell-type selective staining and subsequent imaging of cells were carried out with RGD- and IR800-conjugated SWNTs, solubilized in water by 25% DSPE-PEG(5k)-NH_2 (1,2-distearoyl-*sn*-glycero-3-phosphoethanolamine-*N*-[amino(polyethyleneglycol)] with a M_w of 5000 g mol^{-1}) and 75% C18-PMH-mPEG(90k) (poly(maleic anhydride-*alt*-1-octadecene)methoxy(polyethyleneglycol) with a M_w of 90000 g mol^{-1}). The RGD peptide ligand was linked to the amine groups on the SWNTs to enable selective binding to $\alpha_v\beta_3$-integrin-positive U87-MG cells[34] over the $\alpha_v\beta_3$-integrin-negative MCF-7 cells. Meanwhile, we also covalently attached IR800 dye molecules onto the SWNTs to afford SWNT-

[*] G. Hong, S. M. Tabakman, J. T. Robinson, H. Wang, B. Zhang, Prof. H. Dai
Department of Chemistry, Stanford University
Stanford, CA 94305 (USA)
E-mail: hdai@stanford.edu
Dr. K. Welsher
Department of Chemistry, Princeton University
Princeton, NJ 08544 (USA)
Dr. Z. Chen
State Key Laboratory of Chemo/Biosensing and Chemometrics
College of Biology, Hunan University
Changsha, Hunan, 410082 (China)

[**] This work is supported by the National Institutes of Health–National Cancer Institute (NIH-NCI) (grant number 5R01A135109-02) and the National Science Foundation (NSF) (grant number CHE-0639053).

Supporting information for this article is available on the WWW under http://dx.doi.org/10.1002/anie.201100934.

IR800-RGD conjugates (see Figure 1a and the Supporting Information for experimental details). Upon excitation at 658 nm, the SWNT-IR800-RGD conjugate emitted in the range of 1000 to 1400 nm as a result of the intrinsic bandgap

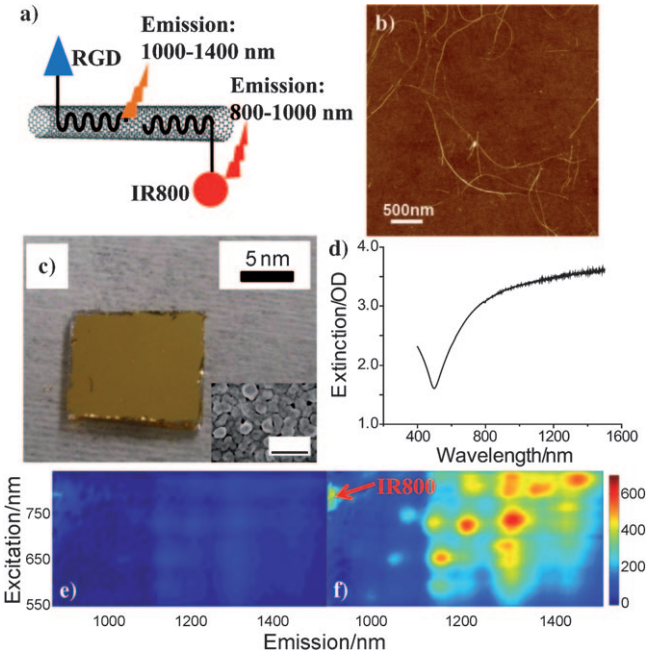

Figure 1. a) The SWNT-IR800-RGD conjugate labeled with the emission ranges of the SWNTs and the IR800 dye. b) An AFM image of SWNT-IR800-RGD conjugates deposited on a quartz substrate. c) A digital photograph of a typical Au/Au substrate used for NIR-FE imaging of cells plated on this substrate. The inset shows an SEM image of the film (scale bar: 500 nm). d) A UV/Vis/NIR extinction spectrum of the Au/Au film. e) A PLE spectrum of SWNT-IR800-RGD conjugates deposited on quartz. f) A PLE spectrum of SWNT-IR800-RGD conjugates deposited on the Au/Au film.

photoluminescence of the SWNTs (Figure 1e and 1f). Upon excitation at 785 nm, the conjugate emitted fluorescence in the range of 800 to 1000 nm due to the attached IR800 molecules (see the "tails" in the short-wavelength region of the emission spectra in Figure 1e and 1f). This unique SWNT-IR800 conjugate tags cells by using two NIR fluorophores in two different imaging windows in the 800 to 1400 nm range. Atomic force microscopy (AFM) imaging (Figure 1b) showed the SWNT conjugates with lengths ranging from 100 nm to 3 μm and an average length of about 1.0 μm.

We synthesized Au/Au films on quartz (Figure 1c) through solution-phase growth (see the Supporting Information) with optimal optical extinction in the NIR (Figure 1d) for the highest fluorescence enhancement of both the SWNTs and IR800 deposited on the gold film (see Figures S1 and S2 in the Supporting Information).[30,35] For the SWNT-IR800-RGD conjugates drop-dried from a solution onto the bare quartz and the Au/Au film on quartz, photoluminescence versus excitation (PLE) spectra revealed fluorescence enhancement of both IR800 (only the emission tail shows up at the upper left corner of Figure 1e and 1f in the spectral range) and the SWNTs (all other peaks in the emission window ranging from 1.0 to 1.4 μm in Figure 1e and 1f) on the Au/Au film. The average enhancement of the SWNT photoluminescence was about ten times, and the enhancement of the IR800 dye attached to the SWNTs was about five times. This result clearly showed the excellent capability of fluorescence enhancement by the Au/Au film for the SWNTs and the IR800 fluorophores emitting in the NIR window ranging from 0.8 to 1.4 μm.

For targeted cell staining and imaging, U87-MG cells and MCF-7 cells were trypsinized and mixed with SWNT-IR800-RGD conjugates at a SWNT concentration of about 30 nM at 4°C for 1 h to prevent endocytosis during the staining. The cells were split into two groups and placed on a quartz microscope slide and the Au/Au film, respectively, for immediate fluorescence imaging using an InGaAs camera (see the Supporting Information for experimental details). The $\alpha_v\beta_3$-integrin-positive U87-MG cells treated with the SWNT-IR800-RGD conjugate showed a ninefold higher SWNT fluorescence signal (green) on the Au/Au film (Figure 2a) than on the quartz slide (Figure 2b) upon excitation at 658 nm under a short exposure time of about 300 ms. Much longer exposure times (1–3 s) were needed to obtain high-quality images of the SWNT-stained cells on quartz, similar to previous biological imaging with SWNT fluorophores.[19,36] The $\alpha_v\beta_3$-integrin-negative MCF-7 cells on both the Au/Au film (Figure 2c) and the quartz slide (Figure 2d) showed little SWNT fluorescence signal. The selectivity of the RGD-SWNT labeling of cells, defined as the ratio of SWNT emission intensity of $\alpha_v\beta_3$-integrin-positive U87-MG cells to that of $\alpha_v\beta_3$-integrin-negative MCF-7 cells, was as high as about 17 for cells on the Au/Au substrate (Figure 2g), and thus higher than the positive/negative ratio of about 7 on quartz, suggesting highly selective staining and molecular imaging of NIR-FE cells on gold films. The cells appeared round-shaped since they were imaged immediately after being placed on the substrates prior to adhesion. To show that these imaged cells were alive during and after imaging, we monitored the U87-MG cells in the cell medium after increasing the temperature to 37°C in a temperature-controlled imaging chamber with a 1 L min^{-1} CO_2 gas flow over a period of 6 h after the first imaging experiment. Both the fluorescence image and the optical image (Figure S3 in the Supporting Information) showed cell adhesion to the Au/Au surface at 37°C, suggesting live cells.

We also trypsinized and mixed cells with SWNT-IR800-RGD conjugates at 37°C (instead of 4°C as mentioned above) for 1 h, conditions known to afford endocytosis of carbon nanotubes inside cells.[37–39] Single-particle tracking of SWNTs in live cells has been studied by Strano and co-workers to reveal the mechanism of endocytosis at 37°C.[40,41] The U87-MG and MCF-7 cells thus treated were plated onto the Au/Au film and the quartz slide for NIR imaging. In contrast to the roughly ninefold enhancement observed for cells stained at 4°C, nanotube fluorescence in the $\alpha_v\beta_3$-integrin-positive U87-MG cells treated at 37°C was enhanced by only about twofold on the Au/Au film (Figure 2h) compared to the enhancement on the quartz substrate

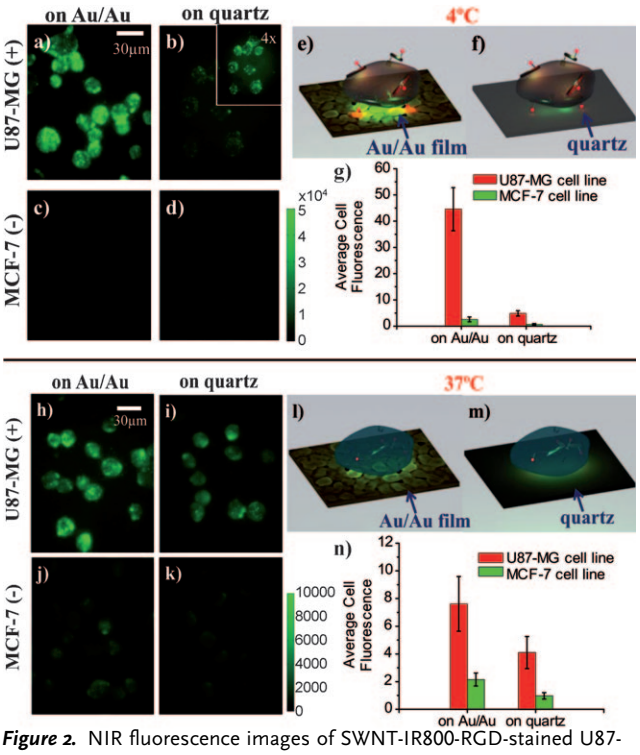

Figure 2. NIR fluorescence images of SWNT-IR800-RGD-stained U87-MG cells at 4 °C a) on the Au/Au film, b) on the quartz substrate, and similarly treated MCF-7 cells c) on the Au/Au film and d) on the quartz substrate. e) The fluorescence of SWNTs sandwiched between a cell membrane and a gold film was enhanced, compared to that of f) SWNT-stained cell on quartz. g) A bar chart showing the average cell fluorescence in (a–d). NIR fluorescence images of SWNT-IR800-RGD-stained U87-MG cells at 37 °C h) on the Au/Au film, i) on quartz, and similarly treated MCF-7 cells j) on the Au/Au film and k) on quartz. l) The fluorescence of SWNTs endocytosed by the cell was hardly enhanced by gold, compared to that of m) SWNT-stained cell on quartz because of the increased distance between the fluorophores and the enhancing gold substrate. n) A bar chart showing the average cell fluorescence in (h–k). All false-colored fluorescence images were recorded under 658 nm excitation with photons collected in the 1100–1700 nm region.

(Figure 2i). Also noticeable was the higher false-positive signal intensity in the $\alpha_v\beta_3$-integrin-negative MCF-7 cells at 37 °C (Figure 2j and 2k), caused by the expected increase of nonspecific uptake of SWNTs by cells over that at 4 °C.

We attributed the fluorescence enhancement of the molecularly selective SWNT labels on the U87-MG cells to coupling between the emissions of the SWNT tags and the surface plasmon modes in the Au/Au substrates. Resonance coupling between SWNT emission and re-radiating plasmonic modes in the Au/Au films shortened the radiative lifetimes of the SWNTs, affording a higher fluorescence quantum efficiency.[30,42,43] It was found that surfactant-coated SWNTs closer to the Au/Au surface exhibited higher fluorescence enhancement, decaying when SWNTs were placed away from the surface with a half-decay distance of about 5 nm,[30] on the same order of cell membrane thickness.[44] At 4 °C, most of the SWNTs were blocked from endocytotic uptake by the U87-MG cells, and the SWNTs on the cell membrane interfacing with the Au/Au substrate were strongly coupled to the surface plasmonic modes in the gold film and thus responsible for the large, roughly ninefold enhanced fluorescence relative to the fluorescence observed on quartz (Figure 2e,f). On the other hand, when incubated at 37 °C, the SWNTs were endocytosed into the cytoplasms of the cells and hence spatially separated from the gold surface, resulting in a reduced fluorescence enhancement of about twofold (Figure 2l,m). We monitored the U87-MG cells stained by the SWNTs at 4 °C in cell medium after increasing the temperature to 37 °C at a CO_2 gas flow of 1 L min^{-1}. We observed an about sixfold decrease of the SWNT fluorescence intensity in the U87-MG cells over time, from the fluorescence intensity recorded right after staining at 4 °C (see Figure S3 in the Supporting Information). This decrease was due to transmembrane endocytosis of the SWNTs at 37 °C, which reduced the NIR-FE effect as the nanotubes were further away from the Au/Au surface. This also confirmed that the cells were fully alive and functioning.

The SWNT–Au distance-dependent fluorescence enhancement could also explain the measured increase in the cellular targeting selectivity with cells on the Au/Au film versus the quartz substrate (Figure 2g). For integrin-negative MCF-7 cells, the fluorescence signals detected were a result of autofluorescence inside the cells and nonspecific uptake effects, which were distributed through the cells in three dimensions. These nonspecific signals were barely enhanced by the Au/Au substrate, while the specific SWNT signals on the integrin-positive U87-MG cells at the cell–gold interface were enhanced to the maximum degree because of their proximity to the Au surface. Thus, the preferential enhancement of specific cell membrane fluorescence afforded more sensitive and selective imaging of the cell membrane receptors. This effect was consistent with little enhancement in the cell labeling selectivity observed on the Au/Au substrate for cells treated by SWNT-RGD at 37 °C (Figure 2n). Interestingly, these results suggested that the distance-dependent fluorescence enhancement effect could be used for tracking transmembrane behavior in live cells, since the thickness of the cell membrane was on the same order of magnitude as the enhancement decay distance (about 5 nm).

Besides the distance dependence of the fluorescence enhancement, another reason for the observed increase in the targeting selectivity on the Au/Au film could be the nonlinearity of the enhancement effect. It was known that surface-enhanced Raman scattering was nonlinear to the concentration, that is, higher concentrations of analytes were usually enhanced more as a result of a better chance to occupy the enhancing "hot spots".[45,46] Therefore, the negative MCF-7 cells were not enhanced as much as the positive U87-MG cells because there were fewer SWNTs on the membranes of the negative cells than on the positive cells, and as a result, the targeting selectivity was magnified by this nonlinear effect.

Our NIR-FE imaging of cells was generally applicable for various NIR fluorescent organic dyes. We chose IR800 as a representative organic dye as it is widely used for biological imaging.[47,48] The IR800 dye molecules (shown as a red circle in Figure 1a) bound to the SWNTs deposited on the same Au/Au film exhibited a fluorescence enhancement by about fivefold (Figure 1e versus 1f). We used SWNT-IR800-RGD conjugates to target $\alpha_v\beta_3$-integrin-positive U87-MG cells and

performed cell fluorescence imaging in the IR800 fluorescence channel. Comparing Figure 3a and 3c corresponding to SWNT-IR800-RGD stained U87-MG and MCF-7 cell lines,

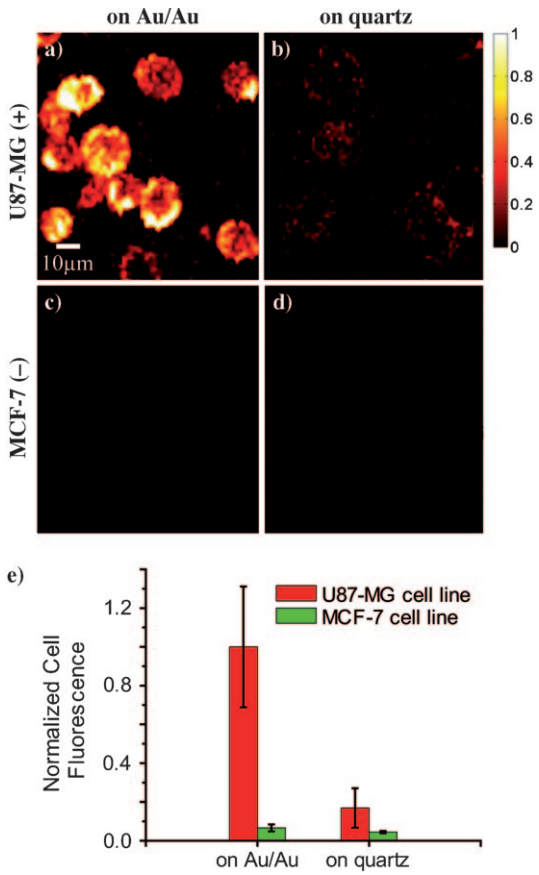

Figure 3. IR800 fluorescence images of SWNT-IR800-RGD-stained U87-MG cells a) on the Au/Au film and b) on quartz, and similarly treated MCF-7 cells c) on the Au/Au film and d) on quartz. Both cell lines were incubated for 1 h at 4 °C. False-colored images were recorded under 785 nm excitation with photons collected in the 790–820 nm region. The bar chart in e) shows normalized cell fluorescence in (a–d).

respectively, the $\alpha_v\beta_3$-integrin-positive U87-MG cells showed a positive IR800 fluorescence signal (red) in the 790 to 820 nm region upon excitation at 785 nm, while the $\alpha_v\beta_3$-integrin-negative MCF-7 cells showed little IR800 signal under the same imaging conditions. This again confirmed the high specificity of the molecular imaging and the coexistence of IR800 and RGD on the SWNTs. Comparison of Figure 3a and 3b revealed a significant fluorescence enhancement on the Au/Au film versus the quartz substrate by about sixfold for the IR800 labels on the cells, with a positive/negative selectivity ratio of about 16 on the Au/Au film versus a ratio of about 4 on the quartz substrate (Figure 3e). These results demonstrated the generality of NIR-FE imaging of cells for high molecular sensitivity and selectivity.

Compared to organic NIR fluorophores, surfactant-solubilized SWNTs exhibit even lower quantum yields ranging from 0.1 to 3%.[13,25,26] Relatively high concentrations of SWNTs (about 60 nM) are typically needed for biological imaging, where the integrin binding sites to RGD on cell membranes are almost saturated.[16] To investigate the detection limit of NIR-FE cell imaging on gold, we labeled $\alpha_v\beta_3$-integrin-positive U87-MG cells by using different staining concentrations of SWNTs ranging from 30 nM to 48 pM and imaged the cells on both the Au/Au film (Figure 4, top

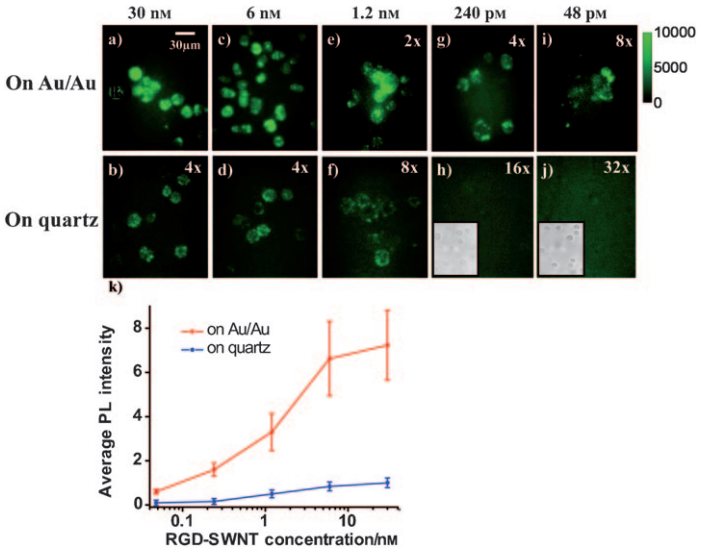

Figure 4. NIR fluorescence images of SWNTs bound to $\alpha_v\beta_3$-integrin-positive U87-MG cells on the Au/Au substrate (top panel) and on quartz (bottom panel), stained with SWNT-RGD conjugates at different concentrations: a,b) 30 nM, c,d) 6 nM, e,f) 1.2 nM, g,h) 240 pM, and i,j) 48 pM. Some of these images with weak fluorescence were autoscaled by a certain multiplier as labeled. Insets in (h) and (j) show the corresponding optical images in the same field of view. All fluorescence images are false-colored. k) The cell titration curves show the average fluorescence intensity of the SWNTs in each stained U87-MG cell on the Au/Au film (red curve) and on quartz (blue curve) at different concentrations of the SWNT-RGD conjugate.

row) and the quartz slide (Figure 4, bottom row). A low detection limit of 1.2 nM SWNT-RGD was reached for labeled cells on the quartz substrate, below which cells (visible in the optical images given in the insets of Figure 4h,j) were hardly discernable in the SWNT fluorescence images. In contrast, on the Au/Au substrates, SWNT fluorescent cell images were observed for cells treated by SWNTs down to a concentration of about 48 pM, suggesting a 25-fold improvement in the detection limit on the Au/Au film (Figure 4k).

In conclusion, we employed plasmonic gold substrates for the first time to perform near-IR-fluorescence-enhanced molecular imaging of cells in the 0.8 to 1.4 μm spectral window based on carbon nanotubes and organic fluorophores. The novel solution-grown gold substrate enhanced the fluorescence of both the carbon nanotubes and the infrared dye IR800 by about nine times and about six times, respectively, affording higher sensitivity and specificity for molecular cell imaging in the advantageous spectral window ranging from 0.8 to 1.4 μm. Cell labeling at different incubation temperatures blocked or allowed endocytosis of

nanotube fluorophores, leading to the observation of a distance-dependent fluorescence enhancement inside the cells. This effect can possibly be used to observe transmembrane behavior of single NIR fluorophores in live cells when the fluorescence enhancement decay distance matches the cell membrane thickness. Further possibilities for NIR-FE imaging include single-molecule imaging and tracking of SWNTs or other NIR dyes on cell membranes, molecular imaging of low-abundance cell membrane proteins, and even some in vivo NIR-FE imaging using smaller Au nanostructures as an enhancing platform to serve in a fluidic system.

Received: February 7, 2011
Revised: March 14, 2011
Published online: April 19, 2011

Keywords: Carbon nanotubes · fluorescence · live-cell imaging

[1] J. V. Frangioni, *Curr. Opin. Chem. Biol.* **2003**, *7*, 626.
[2] V. Ntziachristos, J. Ripoll, R. Weissleder, *Opt. Lett.* **2002**, *27*, 1652.
[3] J. E. Aubin, *J. Histochem. Cytochem.* **1979**, *27*, 36.
[4] Z. Liu, S. Tabakman, K. Welsher, H. J. Dai, *Nano Res.* **2009**, *2*, 85.
[5] Z. Liu, S. Tabakman, S. Sherlock, X. L. Li, Z. Chen, K. L. Jiang, S. S. Fan, H. J. Dai, *Nano Res.* **2010**, *3*, 222.
[6] J. H. Flanagan, S. H. Khan, S. Menchen, S. A. Soper, R. P. Hammer, *Bioconjugate Chem.* **1997**, *8*, 751.
[7] Y. H. Lin, R. Weissleder, C. H. Tung, *Bioconjugate Chem.* **2002**, *13*, 605.
[8] R. Weissleder, C. H. Tung, U. Mahmood, A. Bogdanov, *Nat. Biotechnol.* **1999**, *17*, 375.
[9] V. Ntziachristos, C.-H. Tung, C. Bremer, R. Weissleder, *Nat. Med.* **2002**, *8*, 757.
[10] M. Bruchez, M. Moronne, P. Gin, S. Weiss, A. P. Alivisatos, *Science* **1998**, *281*, 2013.
[11] W. C. W. Chan, S. M. Nie, *Science* **1998**, *281*, 2016.
[12] X. Y. Wu, H. J. Liu, J. Q. Liu, K. N. Haley, J. A. Treadway, J. P. Larson, N. F. Ge, F. Peale, M. P. Bruchez, *Nat. Biotechnol.* **2003**, *21*, 41.
[13] M. J. O'Connell, S. M. Bachilo, C. B. Huffman, V. C. Moore, M. S. Strano, E. H. Haroz, K. L. Rialon, P. J. Boul, W. H. Noon, C. Kittrell, J. P. Ma, R. H. Hauge, R. B. Weisman, R. E. Smalley, *Science* **2002**, *297*, 593.
[14] S. M. Bachilo, M. S. Strano, C. Kittrell, R. H. Hauge, R. E. Smalley, R. B. Weisman, *Science* **2002**, *298*, 2361.
[15] P. Cherukuri, S. M. Bachilo, S. H. Litovsky, R. B. Weisman, *J. Am. Chem. Soc.* **2004**, *126*, 15638.
[16] K. Welsher, Z. Liu, D. Daranciang, H. Dai, *Nano Lett.* **2008**, *8*, 586.
[17] P. Cherukuri, C. J. Gannon, T. K. Leeuw, H. K. Schmidt, R. E. Smalley, S. A. Curley, R. B. Weisman, *Proc. Natl. Acad. Sci. USA* **2006**, *103*, 18882.
[18] T. K. Leeuw, R. M. Reith, R. A. Simonette, M. E. Harden, P. Cherukuri, D. A. Tsyboulski, K. M. Beckingham, R. B. Weisman, *Nano Lett.* **2007**, *7*, 2650.
[19] K. Welsher, Z. Liu, S. P. Sherlock, J. T. Robinson, Z. Chen, D. Daranciang, H. J. Dai, *Nat. Nanotechnol.* **2009**, *4*, 773.
[20] J. T. Robinson, K. Welsher, S. M. Tabakman, S. P. Sherlock, H. L. Wang, R. Luong, H. J. Dai, *Nano Res.* **2010**, *3*, 779.
[21] X. X. Peng, H. X. Chen, D. R. Draney, W. Volcheck, A. Schutz-Geschwender, D. M. Olive, *Anal. Biochem.* **2009**, *388*, 220.
[22] R. Philip, A. Penzkofer, W. Baumler, R. M. Szeimies, C. Abels, *J. Photochem. Photobiol. A* **1996**, *96*, 137.
[23] R. B. Mujumdar, L. A. Ernst, S. R. Mujumdar, C. J. Lewis, A. S. Waggoner, *Bioconjugate Chem.* **1993**, *4*, 105.
[24] D. Magde, R. Wong, P. G. Seybold, *Photochem. Photobiol.* **2002**, *75*, 327.
[25] J. Crochet, M. Clemens, T. Hertel, *J. Am. Chem. Soc.* **2007**, *129*, 8058.
[26] L. J. Carlson, S. E. Maccagnano, M. Zheng, J. Silcox, T. D. Krauss, *Nano Lett.* **2007**, *7*, 3698.
[27] V. Perebeinos, J. Tersoff, P. Avouris, *Nano Lett.* **2005**, *5*, 2495.
[28] M. S. Strano, C. B. Huffman, V. C. Moore, M. J. O'Connell, E. H. Haroz, J. Hubbard, M. Miller, K. Rialon, C. Kittrell, S. Ramesh, R. H. Hauge, R. E. Smalley, *J. Phys. Chem. B* **2003**, *107*, 6979.
[29] S. Y. Ju, W. P. Kopcha, F. Papadimitrakopoulos, *Science* **2009**, *323*, 1319.
[30] G. S. Hong, S. M. Tabakman, K. Welsher, H. L. Wang, X. R. Wang, H. J. Dai, *J. Am. Chem. Soc.* **2010**, *132*, 15920.
[31] E. Le Moal, E. Fort, S. Leveque-Fort, F. P. Cordelieres, M. P. Fontaine-Aupart, C. Ricolleau, *Biophys. J.* **2007**, *92*, 2150.
[32] J. Zhang, Y. Fu, D. Liang, R. Y. Zhao, J. R. Lakowicz, *Langmuir* **2008**, *24*, 12452.
[33] B. Radha, M. Arif, R. Datta, T. K. Kundu, G. U. Kulkarni, *Nano Res.* **2010**, *3*, 738.
[34] Z. Liu, W. B. Cai, L. N. He, N. Nakayama, K. Chen, X. M. Sun, X. Y. Chen, H. J. Dai, *Nat. Nanotechnol.* **2007**, *2*, 47.
[35] S. M. Tabakman, Z. Chen, H. S. Casalongue, H. Wang, H. Dai, *Small* **2011**, *7*, 499.
[36] J. H. Kim, J. H. Ahn, P. W. Barone, H. Jin, J. Q. Zhang, D. A. Heller, M. S. Strano, *Angew. Chem.* **2010**, *122*, 1498; *Angew. Chem. Int. Ed.* **2010**, *49*, 1456.
[37] N. W. S. Kam, T. C. Jessop, P. A. Wender, H. J. Dai, *J. Am. Chem. Soc.* **2004**, *126*, 6850.
[38] N. W. S. Kam, H. J. Dai, *J. Am. Chem. Soc.* **2005**, *127*, 6021.
[39] N. W. S. Kam, Z. Liu, H. J. Dai, *Angew. Chem.* **2006**, *118*, 591; *Angew. Chem. Int. Ed.* **2006**, *45*, 577.
[40] H. Jin, D. A. Heller, M. S. Strano, *Nano Lett.* **2008**, *8*, 1577.
[41] H. Jin, D. A. Heller, R. Sharma, M. S. Strano, *Acs Nano* **2009**, *3*, 149.
[42] H. Mertens, A. F. Koenderink, A. Polman, *Phys. Rev. B* **2007**, *76*, 115123.
[43] J. Gersten, A. Nitzan, *J. Chem. Phys.* **1981**, *75*, 1139.
[44] A. Chen, V. T. Moy, *Biophys. J.* **2000**, *78*, 2814.
[45] Y. Fang, N. H. Seong, D. D. Dlott, *Science* **2008**, *321*, 388.
[46] Z. Chen, S. M. Tabakman, A. P. Goodwin, M. G. Kattah, D. Daranciang, X. R. Wang, G. Y. Zhang, X. L. Li, Z. Liu, P. J. Utz, K. L. Jiang, S. S. Fan, H. J. Dai, *Nat. Biotechnol.* **2008**, *26*, 1285.
[47] K. E. Adams, S. Ke, S. Kwon, F. Liang, Z. Fan, Y. Lu, K. Hirschi, M. E. Mawad, M. A. Barry, E. M. Sevick-Muraca, *J. Biomed. Opt.* **2007**, *12*, 024017.
[48] Y. Chen, S. Dhara, S. R. Banerjee, Y. Byun, M. Pullambhatla, R. C. Mease, M. G. Pomper, *Biochem. Biophys. Res. Commun.* **2009**, *390*, 624.

